Supplementary Material

Ru nanoparticles loaded amorphous CoMoP as an efficient electrocatalyst for alkaline water/seawater hydrogen evolution

Wen-Jing Li [a], Xin-Jie Tian [a], Hai-Yi Sun [a], Xue-Ying Yang [a], Denghao Ouyang [b], Guodong Li [b],

Bin Liu [a, *], Yong-Ming Chai [a], Bin Dong [a,*]

a State Key Laboratory of Heavy Oil Processing, College of Chemistry and Chemical Engineering,

China University of Petroleum (East China), Qingdao 266580, PR China

b PetroChina Shenzhen New Energy Research Institute Co., Ltd., Shenzhen 518052, PR China

* Corresponding author. Email: liubin@upc.edu.cn(B. Liu); dongbin@upc.edu.cn(B. Dong)

Tel: +86-532-86981156, Fax: +86-532-86981156

Experimental section

Acetone (C_3H_6O, ≥99.5 wt.%), hydrochloric acid (HCl 1 M) , and Anhydrous ethanol (C_2H_5OH, ≥99.7 wt.%) was purchased from Shanghai Titan Scientific Co. Ltd., China. Nickel foam (thickness:1.5 mm) were bought from Kunshan Lvchuang Electronic Technology Co. Ltd., China. Cobalt nitrate hexahydrate $Co(NO_3)_2·6H_2O$ (≥98.5 wt.%), potassium hydroxide KOH (≥85.0 wt.%), and Sodium hypophosphite monohydrate $NaH_2PO_2·H_2O$ (98.0～103.0 wt.%) were purchased from Sinopharm Chemical Reagent Co. Ltd., China. Sodium molybdate dihydrate $Na_2MoO_4·2H_2O$ (99.0 wt.%) and Ruthenium (III) chloride anhydrous $RuCl_3$ (45-55 wt.%) was bought from Shanghai Macklin Biochemical Co. Ltd., China. All the experimental chemicals and materials used were of analytical purity and no further post-treatment was required before use.

Materials characterization

The crystal structure of the catalyst was analyzed by X-ray diffraction (XRD), using X 'pert Pro MPD diffractometer Bruker D8 Advance. The scanning electron microscopy (SEM) (Zeiss Sigma 300), transmission electron microscopy (TEM), High-Resolution Transmission Electron Microscope (HRTEM) and Selected area diffraction (SAED) (JEM-2100F, 200 kV) were applied to analyze the morphological structure information of the samples. The element composition and distribute on of the catalysts were characterized by the Energy Dispersive System (EDS) detected on the Zeiss Sigma 300 and JEM-2100F. X-ray photoelectron spectroscopy (XPS) (Thermo Fisher K-Alpha) was used to analyze the composition and valence state of the elements on the surface of the sample.

Electrochemical measurements

All electrochemical tests were performed in the laboratory at room temperature, and the electrolyte solution consisted of 1M KOH and alkaline seawater (1M KOH seawater). The electrochemical workstation used was a Gamry Reference 600 (USA). In the three-electrode system, the sample prepared above, graphite rod and saturated calomel served as the working electrode, counter electrode, and reference electrode, respectively. Linear sweep voltammetry (LSV) was performed at a scan rate of 2 mV s^{-1} from -1 to -1.7 V vs. SCE, and the compensation was corrected by iR (the percentage of compensation was automatically adjusted with the change of the current density value). All the potentials vs. saturated calomel were converted into a standard reversible hydrogen electrode (RHE) by means of the Nernst equation: $E_{RHE} = E_{SCE} + 0.059 pH + 0.243$. The Tafel plots are plotted from the polarization curves with the Tafel equation $\eta = a + blog(j)$, where η is the overpotential, a corresponds to the intercept, b is the Tafel slope, and j is the current density. The cyclic voltammetry (CV) curves were recorded in the non-Faraday region (-0.94 to -1.04 V vs. SCE) at different scan rates ranging from 20 to 100 mV s^{-1} and were used to determine the electrical double-layer capacitances (C_{dl}). The specific calculation equation is as follows:

$$C_{dl} = (ja-jc)/(2 \cdot v) = (ja+|jc|)/(2 \cdot v) = \Delta j/(2 \cdot v)$$

in which ja and jc is the anodic and cathodic voltammetric current density, respectively, recorded at the middle of the selected potential range, and v is the scan rate.

The catalysts were characterized by electrochemical impedance spectroscopy (EIS) at a potential of -1.3 V vs. SCE. Using a frequency range of 100 kHz to 0.1 Hz, EIS Nyquist plots of the as-synthesized samples were measured. In an equivalent electrical circuit, Rs (R_1) stands for solution resistance, CPE for constant phase element and Rct (R_2) for charge transfer

resistance. In addition, the stability of the final sample was tested by a timed potentiometric

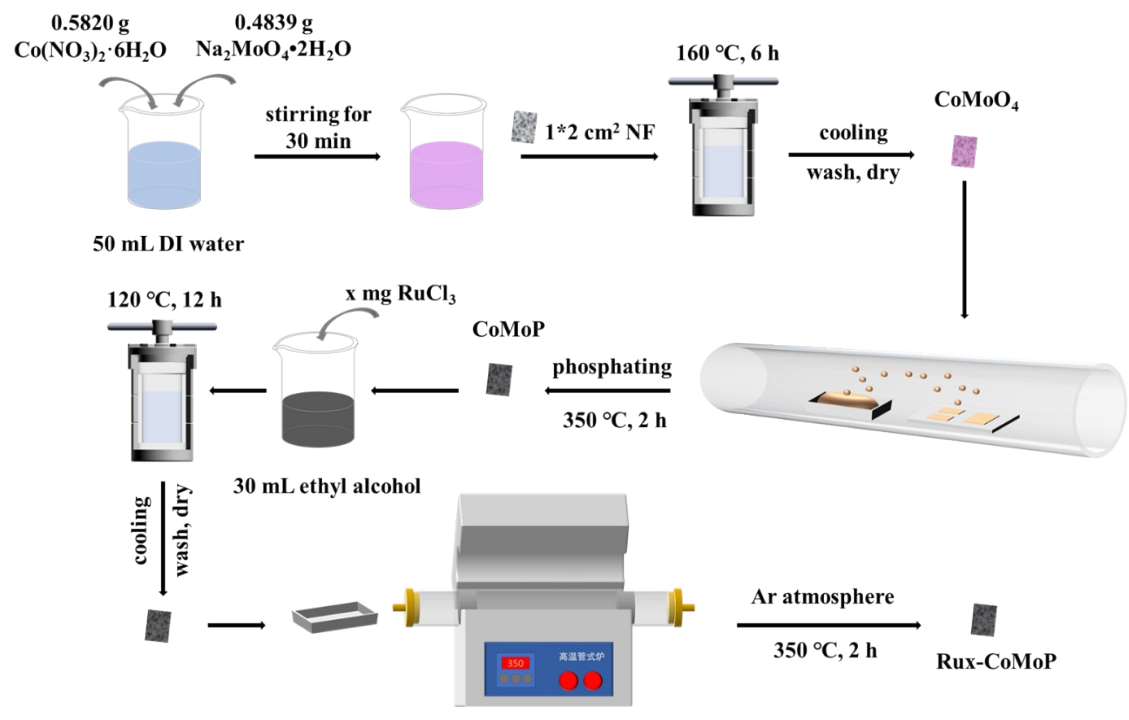method at a current density of 100 mA cm^{-2} for 50 h.

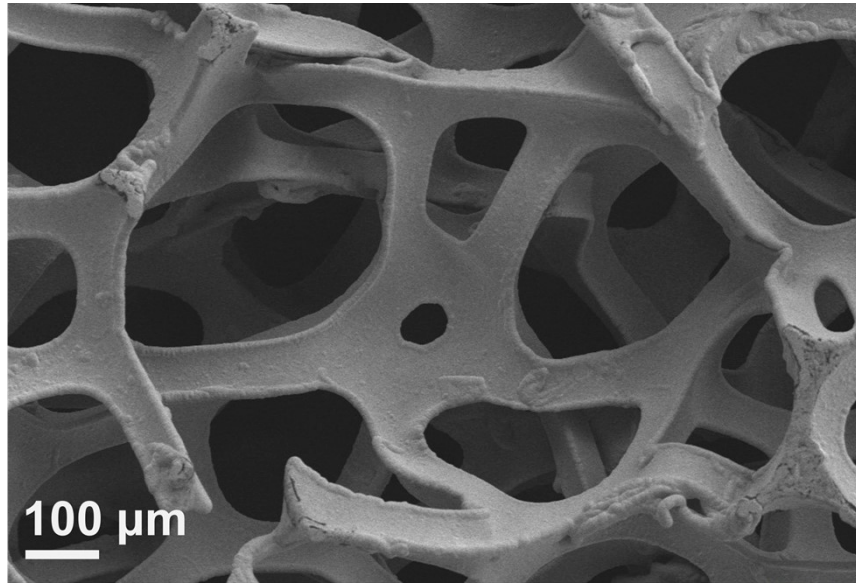**Fig. S1**. The specific synthesis steps of Ru-CoMoP/NF.
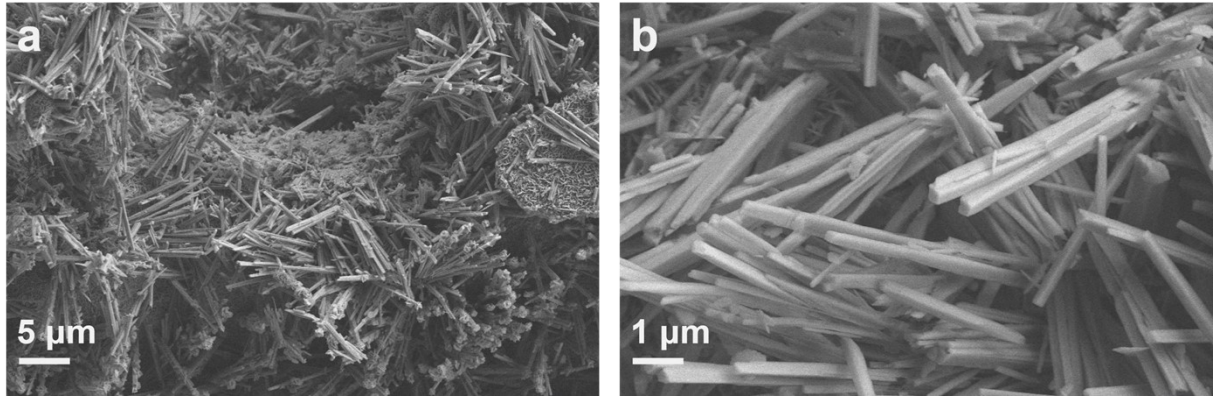
Fig. S2 SEM image of NF.

Fig. S3 SEM image of (a-b) CoMoO$_4$/NF.

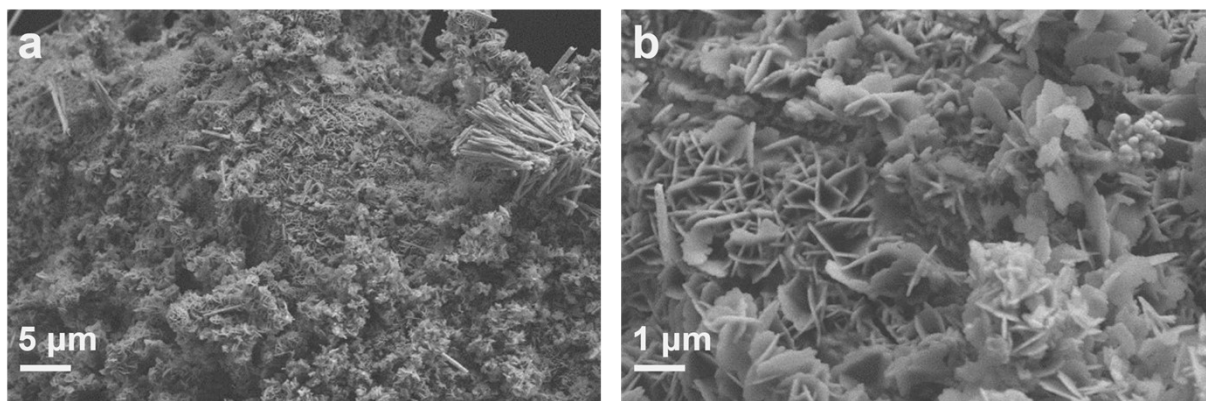**Fig. S4** SEM image of (a-b) CoMoP/NF.
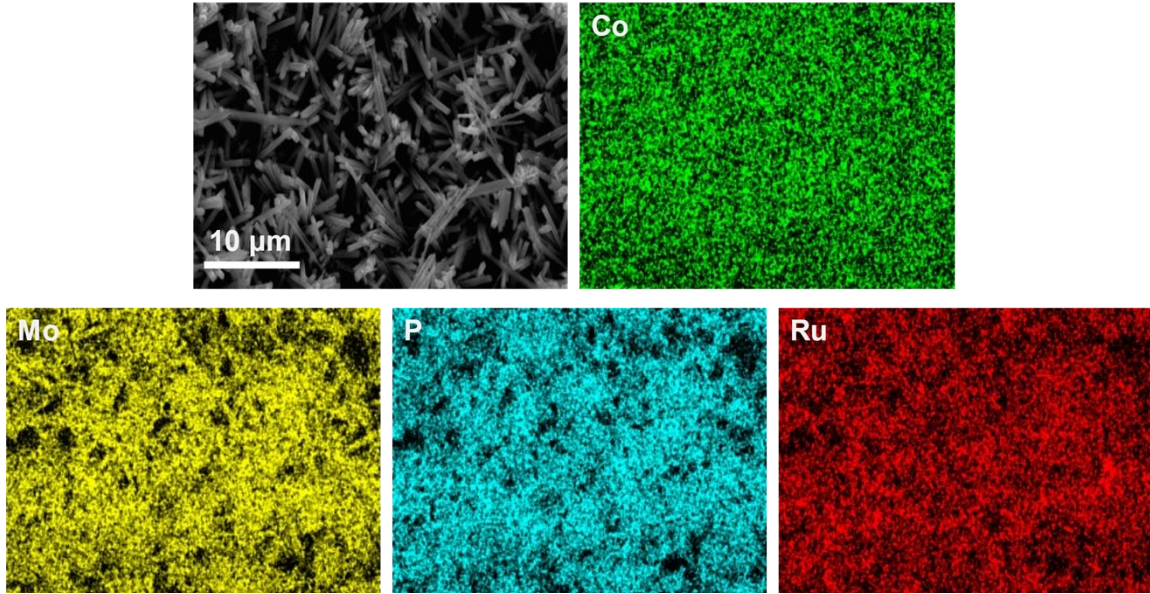
Fig. S5 SEM image and the corresponding elemental mappings of the Ru-CoMoP/NF.

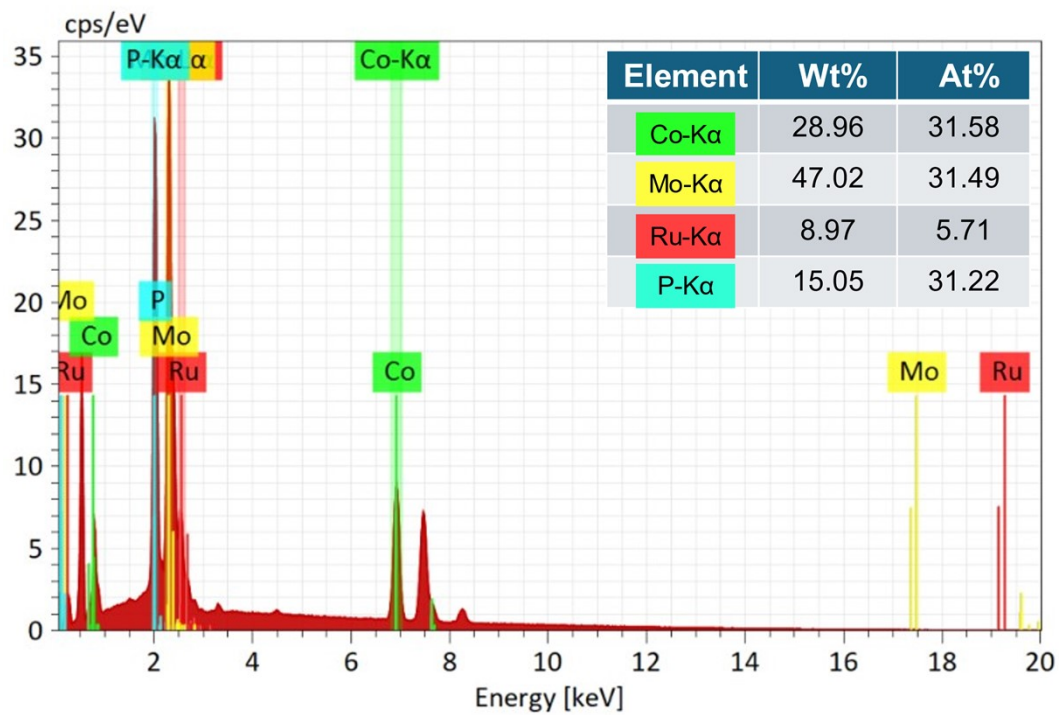| Element	Wt%	At%
Co-Kα	28.96	31.58
Mo-Kα	47.02	31.49
Ru-Kα	8.97	5.71
P-Kα	15.05	31.22

Fig. S6 SEM EDS results of Ru-CoMoP/NF and corresponding element contents.
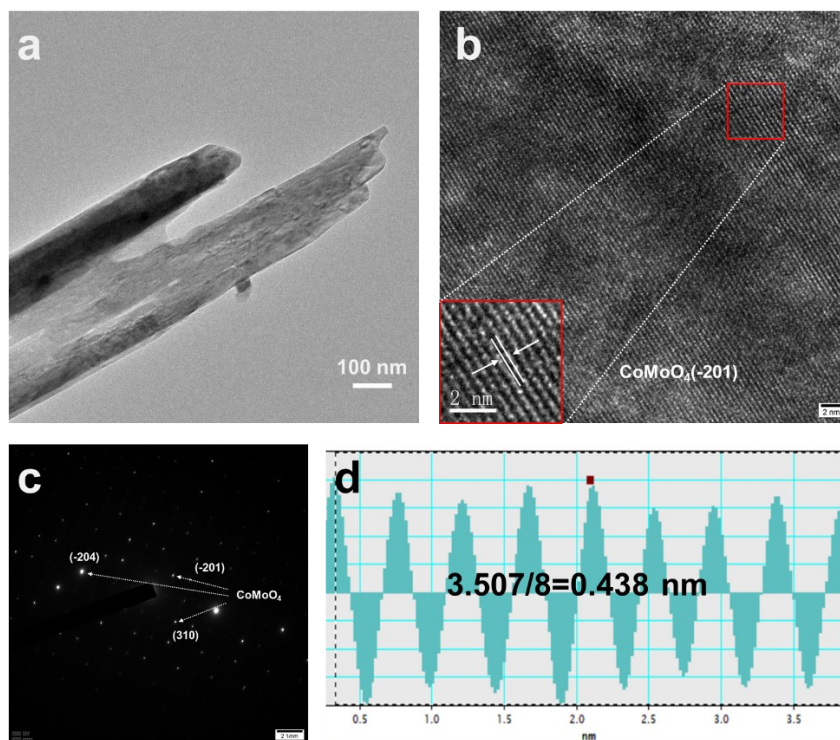
Fig. S7 TEM, HRTEM and SAED image of (a-d) $CoMoO_4$/NF.

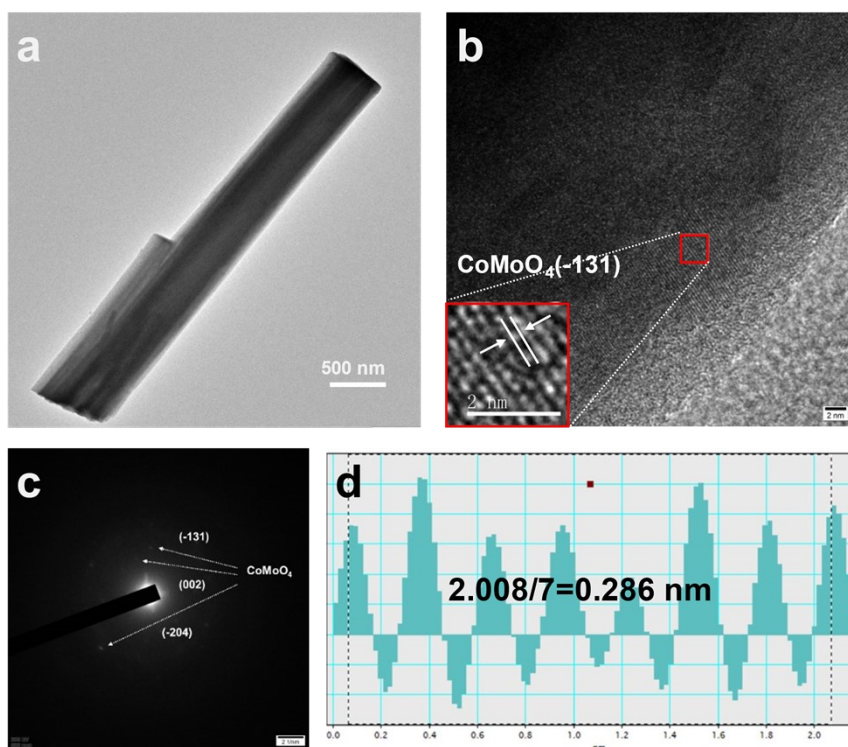**Fig. S8** TEM, HRTEM and SAED image of (a-d) CoMoP/NF.

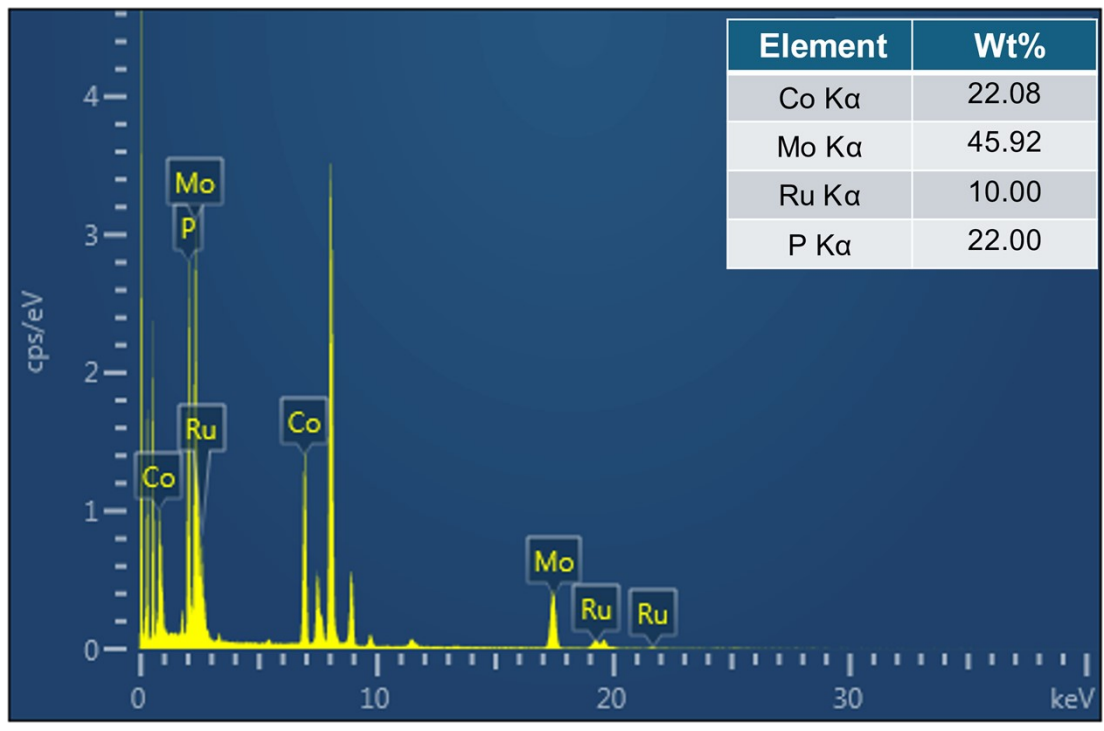| Element	Wt%
Co Kα	22.08
Mo Kα	45.92
Ru Kα	10.00
P Kα	22.00

Fig. S9 HRTEM EDS results of Ru-CoMoP/NF and corresponding element contents.
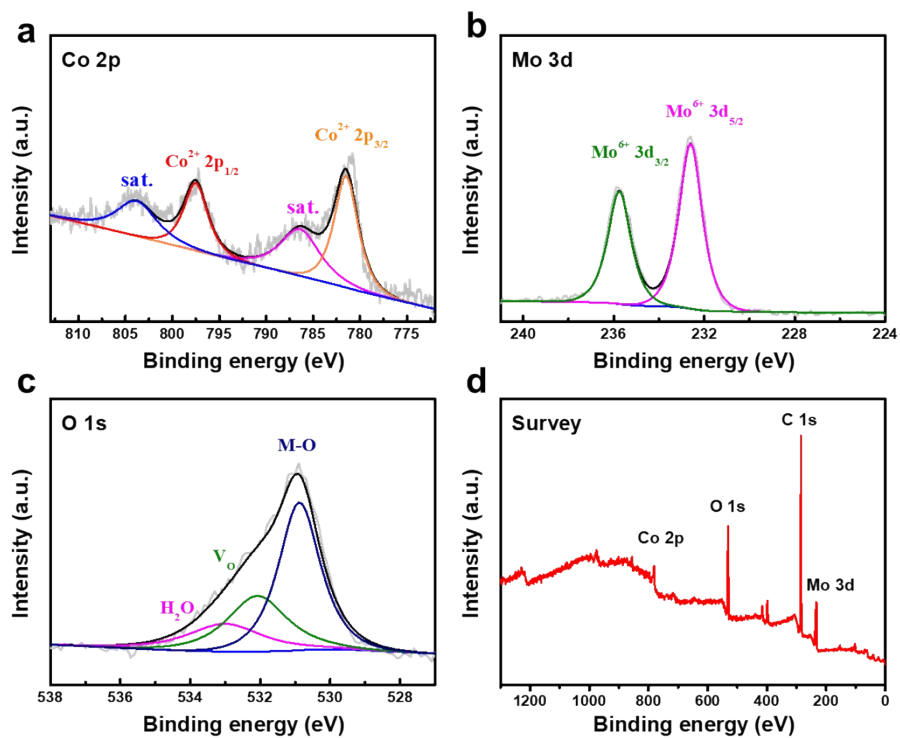
Fig. S10 High-resolution XPS spectra of $CoMoO_4$/NF at (a-c) Co 2p, Mo 3d and O 1s, (d) XPS full survey-scan of $CoMoO_4$/NF.
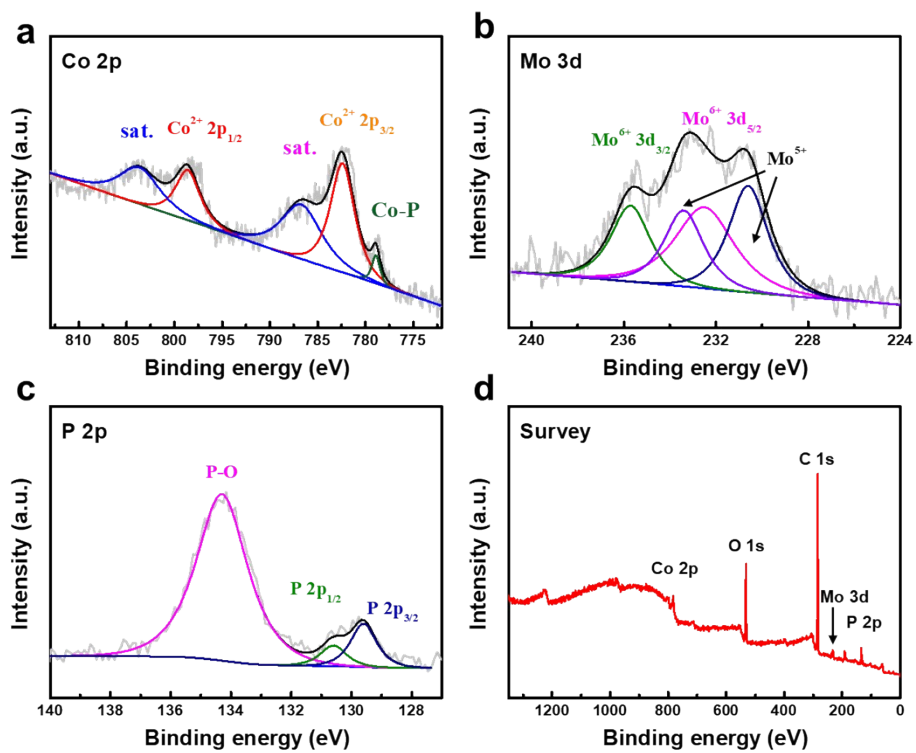
Fig. S11 High-resolution XPS spectra of CoMoP/NF at (a-c) Co 2p, Mo 3d and P 2p, (d) XPS full survey-scan of CoMoP/NF.
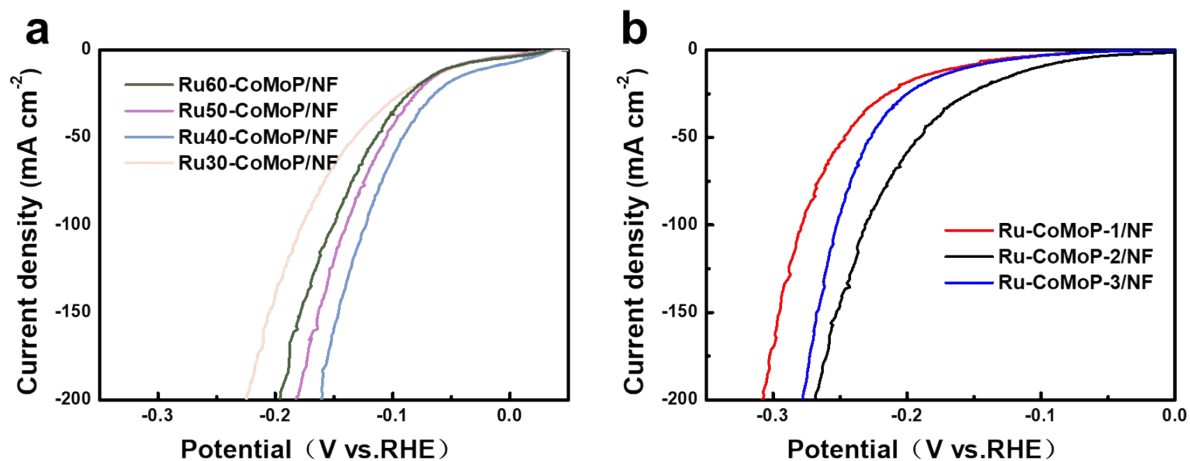
Fig. S12 (a) the polarization curves recorded on Ru$_x$-CoMoP/NF under alkaline media with different RuCl$_3$ mass. (b) the polarization curves recorded on Ru-CoMoP-n/NF under alkaline media with different phosphating times.
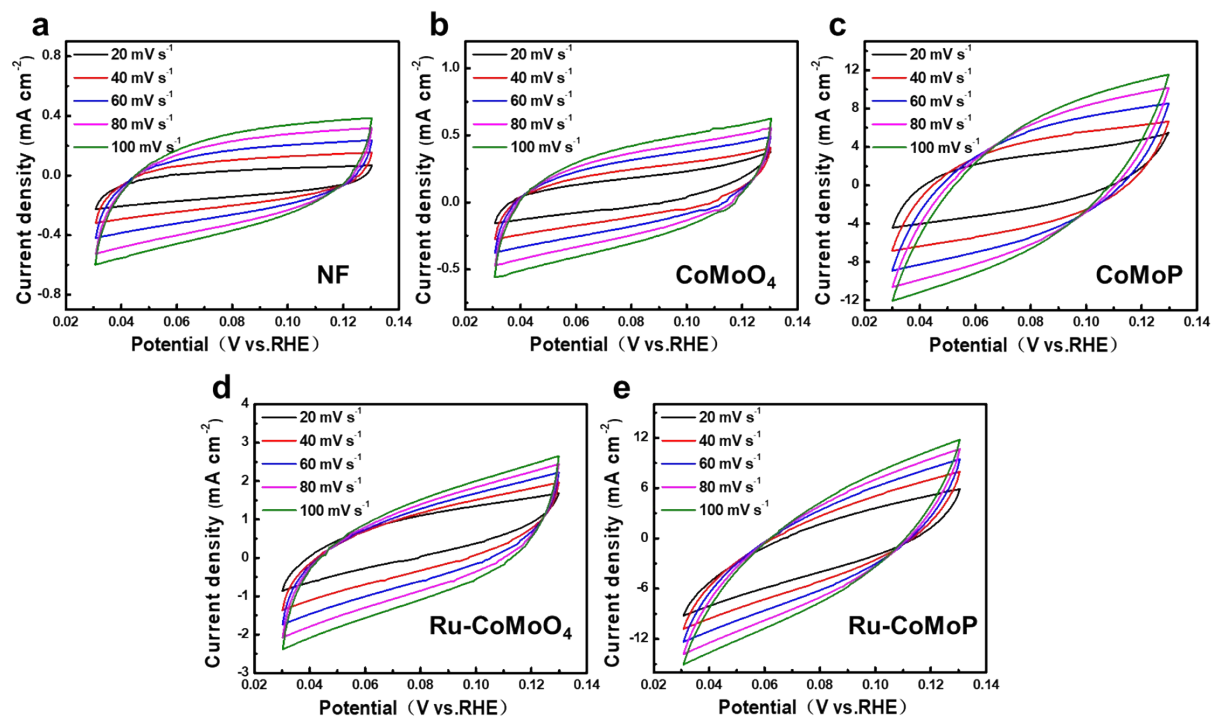
Fig. S13 Cyclic voltammetry curves (CV) of (a) NF, (b) CoMoO$_4$/NF, (c) CoMoP/NF, (d) Ru-CoMoO$_4$/NF and (e) Ru-CoMoP/NF with different scanning rates (20, 40, 60, 80,100 mV s^{-1}) in the potential range of 0.03~0.13 V vs. RHE.

Fig. S14 SEM images of Ru-CoMoP/NF samples after stability test (a) in 1 M KOH, (b) in 1 M KOH seawater.

Table S1 Summary of the Rct values at a potential of -1.3 V vs. SCE in 1.0 M KOH.

	NF	CoMoO$_4$/NF	CoMoP/NF	Ru-CoMoO$_4$/NF	Ru-CoMoP/NF
Rct	7.111	5.363	1.496	1.085	0.629

Table S2 Comparison of HER performance of Ru-CoMoP/NF with other reported catalysts in 1M KOH.

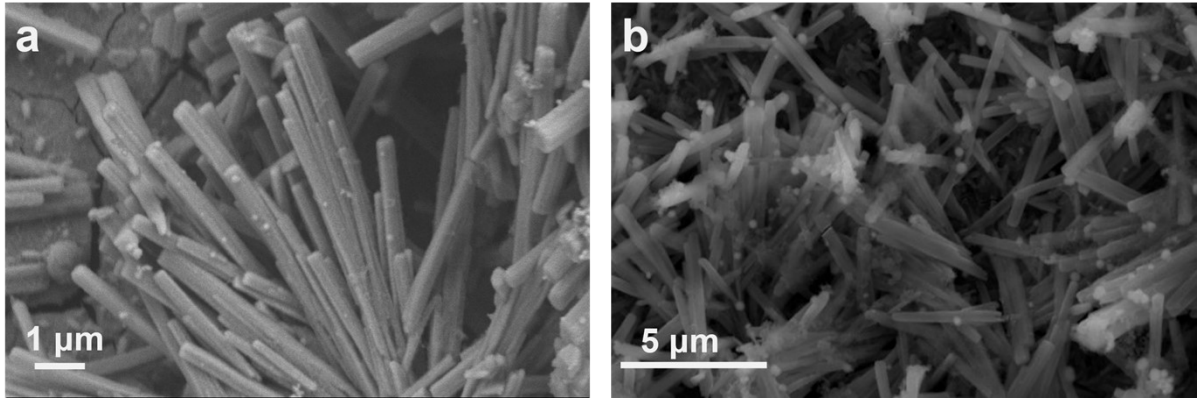| Catalysts	j (mA cm^{-2})	η (mV)	b (mV dec^{-1})	Refer.
Ru-CoMoP/NF	10	18	42.2	**This work**
Ru@FeP$_4$/Fe$_2$PO$_5$	10	49	60.9	[1]
RCFP/NF	10	112	63.3	[2]
Ru-NiMoO$_4$-NF	10	52	45	[3]
Ru-CoP$_x$/NF	10	41	68	[4]
RuV-CoNiP/NF	10	28	49.6	[5]
Ru/NF	10	26.1	55.21	[6]
CoFe-ZLDH/Ru@NF	10	60.9	93.3	[7]
CoRuPO/NF	10	26	97	[8]
Ni$_2$P-Fe$_2$P-Ru$_2$P/NF	10	78.6	85.1	[9]
Ru/CoOOH@NF	10	36	75	[10]

Table S3 Comparison of HER performance of Ru-CoMoP/NF with other electrocatalysts in alkaline seawater (1 M KOH seawater).

Catalysts	j (mA cm^{-2})	η (mV)	Refer.
Ru-CoMoP/NF	10	20	**This work**
CoRuPO/NF	10	62	[8]
RuNi/MoC@NC	10	21	[11]
cRu-Ni$_3$N	10	36	[12]
Ru-NiMoO(P)$_4$	10	37	[13]
β-Ni(OH)$_2$/Ni-Ru SAs NSAs	10	38	[14]
Ru/B-p-FeP$_4$/Fe$_2$P	10	72	[15]
Mo-Ru/CNTs	10	44.9	[16]

Reference

[1] W. Xia, M. Ma, X. Guo, D. Cheng, D. Wu, D. Cao, Fabricating Ru Atom-Doped Novel FeP_4/Fe_2PO_5 Heterogeneous Interface for Overall Water Splitting in Alkaline Environment, *ACS Appl. Mater. Interfaces*, 2023, **15**, 44827-44838.

[2] K. Jang, H. Yoon, J. Hyoung, D. S. A Pratama, C. W Lee, D. Kim, Enhancement of hydrogen evolution activity by tailoring the electronic structure in ruthenium-heteroatom-doped cobalt iron phosphide nanoframes, *Appl Catal B-environ*, 2024, **341**, 123327.

[3] M. Yang, H. Yang, F. Wang, Y. Niu, P. Li, Synergistic effects boosting hydrogen evolution performance of transition metal oxides at ultralow Ru loading levels, *RSC Adv.*, 2023, **13**, 13263-13268.

[4] M. Shang, B. Zhou, D. Liu, M. Yu, Y. Zhang, W. Xiao, P. Yang, G. Xu, Z. Wu, L. Wang, Modulated Co-P bond via ruthenium doping to facilitate spearhead-like CoP_x for overall water splitting, *Int. J. Hydrogen Energy,* 2023, **49**, 15-24.

[5] Q. Ma, H. Jin, F. Xia, H. Xu, J. Zhu, R. Qin, H. Bai, B. Shuai, W. Huang, D. Chen, Ultralow Ru-assisted and vanadium-doped flower-like CoP/Ni_2P heterostructure for efficient water splitting in alkali and seawater, *J. Mater. Chem. A,* 2021, **9**, 26852-26860.

[6] Y. Hou, Z. Qin, X. Han, Y. Liu, W. Zhang, X. Cao, Y. Cao, J. Lang, H. Gu, Thermal evaporation-driven fabrication of Ru/RuO_2 nanoparticles onto nickel foam for efficient overall water splitting, *Nanoscale*, 2024, **16**, 6662-6668.

[7] W. Ning, R. Wang, X. Li, M. Wang, H. Xu, H. Lin, X. Fu, M. Wang, P. Liu, H. Yang, Construction of a ruthenium-doped CoFe-layered double hydroxide as a bifunctional electrocatalyst for overall water splitting, *Chem. Commun.*, 2023, **59**, 11803-11806.

[8] J. Niu, J. Yang, A. Channa, E. Ashalley, J. Yang, J. Jiang, H. Li, H. Ji, X. Niu, Enhancing the water splitting performance via decorating Co_3O_4 nanoarrays with ruthenium doping and phosphorization, *RSC Adv.*, 2020, **10**, 27235-27241.

[9] S. Cai, X. Chen, M. Huang, J. Han, Y. Zhou, J. Li, Interfacial engineering of nickel/iron/ruthenium phosphides for efficient overall water splitting powered by solar energy, *J. Mater. Chem. A*, 2022, **10**, 772-778.

[10] Y. Ma, Y. Ha, L. Chen, Z. An, L. Xing, Z. Wang, Z. Li, Electrochemically Induced Ru/CoOOH Synergistic Catalyst as Bifunctional Electrode Materials for Alkaline Overall Water Splitting, *Small*, 2024, 202311884.

[11] X. Fan, B. Li, C. Zhu, F. Yan, Y. Chen, Regulation of the electronic structure of a RuNi/MoC electrocatalyst for high-efficiency hydrogen evolution in alkaline seawater, *Nanoscale*, 2023, **15**, 16403-16412.

[12] J. Zhu, R. Lu, W. Shi, L. Gong, D. Chen, P. Wang, L. Chen, J. Wu, S. Mu, Y. Zhao, Epitaxially Grown Ru Clusters-Nickel Nitride Heterostructure Advances Water Electrolysis Kinetics in Alkaline and Seawater Media, *Energy Environ. Mater.*, 2023, **6**, e12318.

[13] S. Wu, D. Chen, S. Li, Y. Zeng, T. Wang, J. Zhang, J. Yu, S. Mu, H. Tang, Ru Cluster Incorporated $NiMoO(P)_4$ Nanosheet Arrays as High-Efficient Bifunctional Catalyst for Wind/Solar-To-Hydrogen Generation Systems, *Adv. Sci.*, 2023, **10**, 2304179.

[14] P. Yan, T. Yang, M. Lin, Y. Guo, Z. Qi, Q. Luo, X. Yu, "One Stone Five Birds" Plasma Activation Strategy Synergistic with Ru Single Atoms Doping Boosting the Hydrogen Evolution Performance of Metal Hydroxide, *Adv. Funct. Mater.*, 2023, **33**, 202301343.

[15] Z. Wang, P. Yang, D. Liu, W. Jin, W. Xiao, Z. Xiao, Z. Wu, L. Wang, Amorphous Ru Coupled with Defect-Abundant B-Doped FeP_4/Fe_2P Porous Nanospheres as an Electrocatalyst for Hydrogen Generation with a Wide pH Range, *ACS Appl. Nano Mater.*, 2023, **6**, 19905-19914.

[16] J. Sun, Z. Zhao, Z. Li, Z. Zhang, R. Zhang, X. Meng, Ultrafast carbothermal shocking fabrication of cation vacancy-rich Mo doped Ru nanoparticles on carbon nanotubes for high-performance water/seawater electrolysis, *J. Mater. Chem. A*, 2023, **11**, 22430-22440.